International Journal of Applied Earth Observation and Geoinformation 30 (2014) 65–75

Contents lists available at ScienceDirect

International Journal of Applied Earth Observation and Geoinformation

journal homepage: www.elsevier.com/locate/jag

Development of an invasive species distribution model with fine-resolution remote sensing

Chunyuan Diao, Le Wang*

Department of Geography, University at Buffalo, The State University of New York, 105 Wilkeson Quad, Buffalo, NY 14261, USA

ARTICLE INFO

Article history:
Received 19 August 2013
Accepted 31 January 2014
Available online 22 February 2014

Keywords:
Saltcedar
Species distribution model
Fine scale
Harmonic analysis
Spatial autocorrelation
Remote sensing

ABSTRACT

Saltcedar (*Tamarix* spp.) is recognized as one of the most aggressively invasive species throughout the Western United States. Mapping its suitable habitat is of paramount importance to effective management, and thus, becomes a high priority for conservation practitioners. In previous studies, species distribution models (SDMs) have been applied to predicting the suitable habitats of saltcedar at national scale, but at coarser spatial resolution (1 km). Although such studies achieved some success, they are lacking of capability to accommodate fine-scale resolution environmental variables, and therefore, fail to uncover detailed spatial pattern of habitats. The objective of this study was to develop a remote sensing driven SDM so as to characterize suitable habitats of saltcedar at very fine spatial scale (30 m). We exploited several fine-scale environmental predictors through remote sensing images, and utilized the logistic regression model to analyze the species–habitat relationship by identifying influential factors with subset selection criteria. We also incorporated the spatial autocorrelation with regression kriging method. Our results indicated that the model incorporating spatial autocorrelation achieved a higher accuracy than that of regression only model. Among 10 environmental variables, the distance to the river and the phenological attributes summarized by the harmonic analysis were regarded as the most significant in predicting the invasive potential of saltcedar. We conclude that remote sensing driven SDM has potential to identify the suitable habitat of saltcedar at a fine scale and locate appropriate areas at high risk of saltcedar infestation, which could benefit the early control and proactive management strategies to a large extent.

Published by Elsevier B.V.

1. Introduction

The invasion of exotic plants has posed significant threat to the species diversity and caused substantial economic damages at the global scale (Ficetola et al., 2007). Saltcedar (*Tamarix* spp.), an exotic woody shrub, is particularly problematic in the southwestern United States through replacing the native vegetation and depleting the river flow (Carruthers and Deloach, 2004). Along with the increasing availability of remotely sensed images, a suite of classification methods have been developed for successfully differentiating the saltcedar from native vegetation at different spatial scales (Everitt and Deloach, 1990; Groeneveld and Watson, 2008; Hamada et al., 2007; Silván-Cárdenas and Wang, 2010; Wang et al., 2013). However, these methods are mostly attempting to map the presence and abundance of established mature saltcedar with plant spectral characteristics, but are lacking capacity to predict the potential distribution of saltcedar in areas where invasion has not occurred. On the other hand, identification of potential invasive susceptible areas, particularly during the early stage of infestation, will allow resources managers to develop cost-effective control strategies. To this end, it is desired to develop appropriate methods for predicting suitable habitats of saltcedar with the integration of remote sensing and other auxiliary information.

Species distribution models (SDMs), based on the niche concept, are increasingly used to detect the spatial pattern and predict the early invasion of exotic plants by investigating the relationship between species occurrence and environmental gradients (Elith and Leathwick, 2009). By highlighting the priority susceptible locations and identifying the potential extent of infestations, SDMs can greatly assist land managers in coordinating response for effective eradication of exotic plants before they become widely established and costly to contain (Kerns et al., 2009). In recent studies, SDMs were employed for mapping the saltcedar habitat suitability at the national scale by relating the field occurrence data with land cover, topo-climatic and vegetation information (Cord et al., 2010; Jarnevich et al., 2011; Morisette et al., 2006). These studies successfully predicted the areas susceptible to saltcedar invasion and also demonstrated that the range of suitable habitat of saltcedar is much wider than that is currently invaded. However, due to the relatively coarse spatial resolution (1 km), these studies aimed at mapping the national-scale habitat of saltcedar and evaluating the relative

* Corresponding author. Tel.: +1 716 645 0474; fax: +1 716 645 2329.
E-mail addresses: chunyuan@buffalo.edu (C. Diao), lewang@buffalo.edu (L. Wang).

0303-2434/$ – see front matter. Published by Elsevier B.V.
http://dx.doi.org/10.1016/j.jag.2014.01.015

ranking of habitat suitability, but not for predicting the sporadic and heterogeneous pattern of early invasion process, or assessing the absolute probability of the habitat. Accordingly, the national-scale risk mapping is still difficult for land managers to locate appropriate areas at high risk of infestation beneficial to further ground-based reconnaissance. Fine scale mapping of habitat suitability, on the other hand, can uncover the detailed spatial pattern of habitats and quantify the spatial heterogeneity of ecological structures (Borcard and Legendre, 2002; Engler et al., 2004; Gottschalk et al., 2011). As the scale becomes finer, the geographic patterns of distribution become patchier and the overall landscape fragmentation increases (Del Barrio et al., 2006). Sporadic and sparse patches undetected at the coarse scale become more distinguishing and more probable to be captured. Consequently, fine-scale mapping of suitable habitats can dramatically help local land governors investigate the invasive potential of nonnative species in the early stage and develop the corresponding control methods for saltcedar infestations in specific local areas. Despite the extensive studies on SDMs, yet fine-scale mapping is poorly explored and understood (but see Andrew and Ustin, 2009; Evangelista et al., 2008).

Compared to the coarse scale mapping, this noted dearth of research at fine scale is mostly attributable to three critical issues: the relative importance of environmental predictors, the influence of spatial autocorrelation and the accessibility of ample samples. Bioclimatic factors, such as temperature and precipitation, have proven to play a pivotal role in mapping the coarse-scale habitat suitability of saltcedar (Friedman et al., 2005; Jarnevich et al., 2011). However, variables that are previously proven effective at coarser resolution may not preserve significance at higher spatial resolution (Menke et al., 2008). Besides, spatial autocorrelation, as a measure of dependency among spatial observations, becomes more prominent at a finer scale. Hence, incorporating the spatial information becomes imperative for achieving an accurate prediction result. Finally, the number of samples required for training and validation of SDM will grow drastically at the fine scale and field campaign may not be an effective method for collecting adequate samples. Remote sensing images, with the scale flexibility, not only enhance the chance of selecting appropriate fine-scale environmental predictors, but also provide an expedient means to obtain the detailed saltcedar information, and hence more flexible and randomized occurrence records. For that reason, our study hypothesized that remote sensing images can facilitate the fine-scale habitat mapping by deriving continuous spatial measurements of both environmental variables and occurrence data.

The objective of the research is to develop a remote sensing driven SDM method at a fine scale that articulates the aforementioned three critical issues. The specific objectives are to: (1) extract appropriate fine-scale environmental predictors from remote sensing images for analyzing the species–habitat relationship, (2) assess the role of environmental predictors in determining the habitat suitability of saltcedar, (3) test whether the incorporation of spatial autocorrelation can lead to increased accuracy in estimating the saltcedar suitable habitats, and (4) evaluate the performance of fine-scale SDM by monitoring the dynamic change of saltcedar.

2. Study area and data

2.1. Study area

The study site (Fig. 1) is located along the Forgotten River reach of the Rio Grande River near the town of Candelaria, Texas, USA (104.69° W, 30.14° N). The Rio Grande River is the third longest river in the continental U.S. and the major tributary, the Rio Conchos, supplies most of the water in the Texas-Mexico border. The climate of this riparian zone is semi-arid to arid with average annual precipitation less than 30 cm and average temperature around 32 °C. The study area is about 4 km by 10 km with the topography characterized by canyons and small valleys. The elevation of this segment ranges from 700 m to 1150 m. The vegetation on both banks of the river is composed mostly of saltcedar (*Tamarix chinensis* L.) with some mixes of willow (*Salix* spp.) and mesquite (*Prosopis* spp.). The native cottonwood (*Populus* spp.), that once dominated the area, is completely absent (Silván-Cárdenas and Wang, 2010). The infestation of saltcedar varies in density and extent, partly due to differences in the local hydrologic system, ranging from individual trees to large continuous patches.

2.2. Image acquisition and pre-processing

2.2.1. Occurrence data

Due to the paucity of fine-scale samples with high locational accuracy in our study area, we attempted to acquire the occurrence data of saltcedar from high resolution Airborne Imaging Spectroradiometer for Applications (AISA) imagery. The AISA imagery had 61 bands in the spectral range 400–1000 nm and the spatial resolution was 1 m. It was acquired on December 21, 2005, which coincided with the time window when saltcedar leaves turn a yellow-orange to orange-brown color and thus can be distinguished from native willow and mesquite species more easily (Everitt and Deloach, 1990).

In order to acquire the occurrence data of saltcedar, we classified the AISA image with Spectral Angle Mapper (SAM) method (Kruse et al., 1993), which compares the image spectra to the reference spectra (endmembers) in the spectral library via the spectral angle and classifies the image spectra as the class with the smallest angle. Two field campaigns were conducted in November 2004 and December 2005 to collect sufficient ground reference samples. With a handheld GPS unit, we recorded the location of saltcedar, native woody riparian species, non-woody vegetation and other land cover types. In total there were forty-two points and thirty polygons. Point features were measured near the trunk of trees by lifting the GPS antenna up to 4 m with a telescoping pole. Additional polygons for non-vegetated land cover classes were selected directly from AISA image based on on-screen visual interpretation. A classification system encompassing the most important land cover types (twelve classes, see Fig. 2) in the study site was then designed. The sample size of these classes varied but all values fell between 90 pixels (for poverty weed) and 312 pixels (for saltcedar). For each class, 50% of samples were randomly selected for training the model and the remainder were reserved for testing. The SAM classification result was shown in Fig. 2. The overall accuracy of the classification result calculated from the testing samples was 82.5% and the kappa coefficient was 0.81. For the saltcedar class alone, the producer's accuracy was 89.3% and the user's accuracy was 94.2%. SAM classification result was resampled to 30 m resolution for maintaining the same scale with that of environmental layers, and the fraction of saltcedar was calculated. Given the classification accuracy of AISA imagery, the approximate error of the resulted saltcedar fractions was about 10%.

At the 30 m scale, the pixel with its fraction of saltcedar greater than 10% was labeled as the presence point, otherwise it was taken as the absence point. We selected 10% as the threshold in order to take into account the error of the aggregated saltcedar fractions introduced by the classification procedure. Compared to the majority rule, this partition of occurrence data is more likely to meet the pixel-based equilibrium assumption of correlative modeling of species' distributions. With the classification result of saltcedar and others, 400 presence points and 400 absence points were randomly

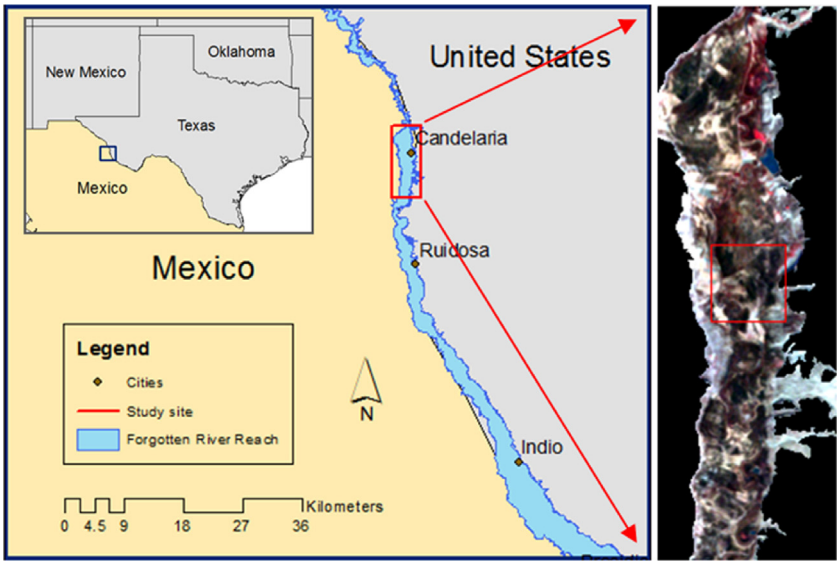

Fig. 1. Geographic location of the study site, false-color composite of Landsat imagery with red color indicating vegetation area.

generated. The data were then divided into training and testing sets using a 75:25 split following a heuristic suggested by Fielding and Bell (1997) for presence/absence data with more than ten predictor variables. Accordingly, for each category, 300 points were used for training the model, while 100 points were reserved for validation.

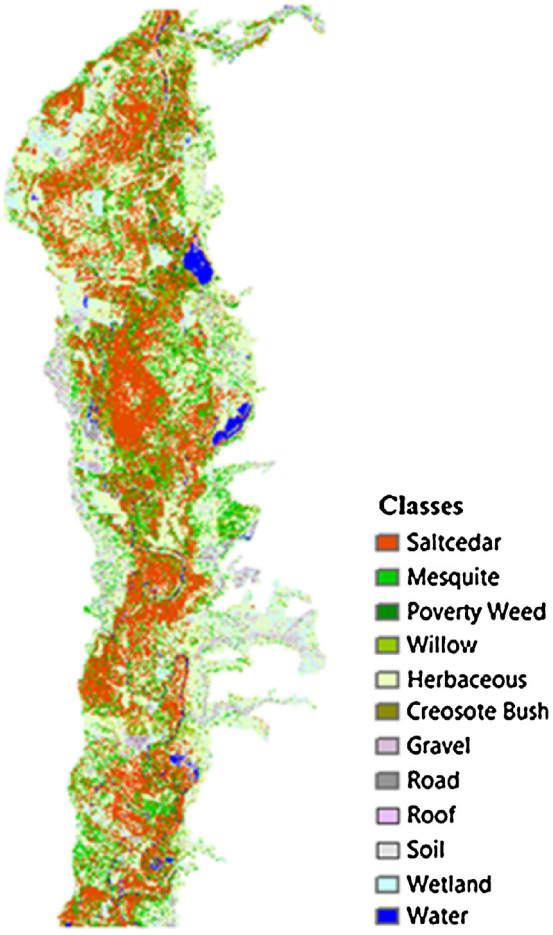

Fig. 2. SAM classification result of high resolution AISA imagery.

2.2.2. Environmental data

From previous studies, the mean annual minimum temperature (Friedman et al., 2005), the mean temperature of the warmest quarter (Jarnevich et al., 2011), the precipitation of the warmest quarter (Cord et al., 2010) have been regarded as the most significant bioclimatic factors in predicting the habitat suitability of saltcedar at the coarse scale, however these factors remain relatively invariant and exhibit high spatial autocorrelation at the fine scale (30 m). Therefore, local environmental predictors, which can uncover the detailed spatial pattern of habitats and quantify the spatial heterogeneity, should be fully investigated.

We attempted to derive these predictors from remote sensing images, namely 30 m resolution Landsat TM images, since these relatively high resolution imagery not only can help us detect the detailed spatial pattern of saltcedar, but also can dramatically facilitate the generalization of fine-scale mapping of suitable habitats. The pixel-based environmental predictors we selected include phenological attributes, vegetation indices and topographical features with more specific reasons explained below.

Phenological attributes, as measures of vegetation phenology, greenness and thermal seasonality, can be used to distinguish the invasive species from associated native vegetation by characterizing the unique temporal-spectral signature of species. Remotely sensed time-series vegetation indices are increasingly utilized to exploit subtle phenological differences, identify the temporal trends as well as map the suitable habitats of saltcedar. In previous studies, MODIS time-series NDVI/EVI phenological metrics have been regarded as significant in detecting the potential habitats of saltcedar at the coarse scale (Cord et al., 2010; Morisette et al., 2006), and time series analysis has been proven more efficient in distinguishing phenological differences between saltcedar and native species than the single-scene analysis (Evangelista et al., 2009). Accordingly, we selected the pixel-based phenological attributes, including the time-series NDVI mean, amplitude and phase, as the environmental predictors (Details can be found in Section 3.1). Despite the temporally continuous availability of MODIS data, the coarse spatial resolution (250 m) of MODIS data cannot detect the detailed spatial pattern of saltcedar and is thus inadequate for the fine-scale mapping. To resolve this issue, we attempted to retrieve the phenological characteristics from monthly Landsat TM images with 30 m spatial resolution. Correspondingly, 32 Landsat TM images (path 31, row 39) from 2004

to 2006 were selected for their seasonal variation with the cloud coverage less than 10%. Four images were highly contaminated by cloud shadow and they were interpolated by averaging the images of adjacent months. In total, there were 36 images during three-year period with one image in each month.

Vegetation indices, including the single-scene NDVI and Tasseled Cap Wetness, were also selected as environmental predictors in our study. The AISA image, which was acquired on December 21, 2005, was resampled to 30 m for calculating the NDVI, since saltcedar's foliage turns an orange-brown color at that time and can be discriminated from native species more easily (Everitt and Deloach, 1990). By quantifying the photosynthetic capacity of plant canopies, NDVI can be employed to detect the change in saltcedar foliage. Additionally, we selected the Landsat TM scene on June 18, 2005 to calculate the Tasseled Cap Wetness, which has been shown useful in identifying the species composition and structure (Cohen et al., 1995; Jin and Sader, 2005), as well as mapping the spatial distribution of saltcedar (Evangelista et al., 2009).

All Landsat TM images were co-registered to the reference image with RMSE less than 0.2. The reference image was derived by spectrally filtering the AISA image and spatially resampling the image to match the resolution of Landsat TM images. Corresponding to the spectral range of AISA image, bands 1–4 of Landsat TM images were selected in our study and they have been proven efficient in detecting the saltcedar (Everitt and Deloach, 1990). Subsequently, the radiometric calibration and normalization were employed to eliminate the atmospheric effect of Landsat images using the iteratively re-weighted multivariate alternation detection (IR-MAD) method (Canty and Nielsen, 2008; Nielsen, 2007) based on the reference image. The IR-MAD method can detect pseudo invariant features automatically and conduct an orthogonal linear transformation on a pair of images. The extension of IR-MAD in ENVI was implemented for the radiometric correction in this study (Canty, 2007).

Finally, topographical features, including the distance to the river, elevation and slope, were selected as environmental variables for characterizing the physical landscape in our fine-scale mapping, since the germination of saltcedar requires the extended moisture and the establishment mainly occurs along the river banks with gentle slopes (Di Tomaso, 1998; Warren and Turner, 1975). Besides Zavaleta and Royval (2002) found that the expansion rate of saltcedar is limited by local elevation and it spreads very slowly after 1220 m. In order to produce an accurate model of the subsequent fine-scale mapping, we extracted the main river channel in our study area from the AISA imagery using Spectral Angel Mapper Target Finder method in ENVI. By setting a continuum of maximum angel thresholds, we chose the optimal one to delineate the river from the image. The distance to the river was then calculated using the Euclidean distance of spatial analyst in ArcGIS with the cell size of 30 m. The digital elevation model (DEM) of 30 m resolution was acquired from the USGS national elevation dataset, and slope was calculated based on the DEM using the surface analysis function of 3D analyst in ArcGIS.

Overall, environmental layers in our study were comprised of both remote sensing and topographical data. With regard to the remote sensing layers, we selected the NDVI time-series phenological attributes (mean, amplitude and phase), the NDVI on December 21, 2005 and the Tasseled Cap Wetness on June 18, 2005. Among the topographic features, we chose elevation, slope and the distance to the river. These layers were selected after we tested and removed the highly correlated layers.

3. Methods

This section summarizes the methods utilized in this study. A flow chart of the major methods were shown in Fig. 3. We first employed harmonic analysis (Section 3.1) to exploit the phenological characteristics of saltcedar and associated native vegetation. Next, we introduced one of the classic SDMs, logistic regression (Section 3.2), for investigating the relationship between occurrence data and environmental estimates. Additionally, we presented regression kriging method (Section 3.3) so as to incorporate the spatial autocorrelation in our fine-scale mapping. Finally, we introduced the validation method in this study and provided some new insights for testing the validity of SDMs (Section 3.4).

3.1. Harmonic analysis

36 monthly Landsat TM images (path 31, row 39) acquired during the three-year period were utilized to generate average annual time series NDVI curves for extracting the phenological attributes (mean, amplitude and phase) of saltcedar and native vegetation through harmonic analysis (Jakubauskas et al., 2001; Moody and Johnson, 2001; Roerink et al., 2000).

As the core of harmonic analysis, Discrete Fourier Transform (DFT) was utilized in our study to decompose the temporal curve to the frequency domain as the sum of a series of harmonic sine and cosine waves (Briggs and Henson, 1995). Each wave designates unique cycle over the defined interval and is denoted by peculiar amplitude and phase value, where amplitude represents half the height of the wave and phase defines the offset between the origin and the peak of the wave. The unique decomposed wave accounts for the percentage of the overall variability of the original time-series curve. Subsequently, inverse Fourier transform was employed to convert the information in the frequency domain back to the temporal domain. DFT requires the equal sampling rate within the temporal domain and is shown in Eq. (1).

$$f(x) = a_0 + \sum_{n=1}^{\infty} \left(a_n \cos \frac{n2\pi x}{N} + b_n \sin \frac{n2\pi x}{N} \right) \quad (1)$$

Here N is the number of samples in the times series, which equals 12 in our study for representing the monthly sampling rate. a_0 is the mean, a_n and b_n are the n-order trigonometrics. Each order represents a harmonic and designates a unique cycle, such as when n equals one, a_1 and b_1 are the first-order trigonometrics, and the decomposed wave is unimodal with only one cycle (Moody and Johnson, 2001). Six harmonics will be produced by DFT with 12 samples. We only considered the first three harmonics, which explained most of the variability in the original time-series curve.

Based on Discrete Fourier Transform, Harmonic Analysis of Time Series (HANTS) algorithm (Roerink et al., 2000) was implemented in our study to extract the phenological profile of vegetation. Advantages of HANTS include its insensitivity to the cloud contamination and extreme pixels, and thus it can dramatically improve the performance of DFT. The HANTS algorithm compares the observed value with the predicted value iteratively, removes the data surpassing the invalid data rejection threshold, and interpolates these data by fitting the weighted least square curve. The range for detecting the outliers, the maximum invalid points, the number of frequencies and the maximum iteration times can also be set for the HANTS algorithm.

The mean, amplitude and phase, extracted by HANTS, were regarded as meaningful and important in mapping the habitat suitability owing to the phenological interpretation. The mean NDVI represents the overall greenness and productivity, and can differentiate the unproductive areas from highly productive ones. The amplitude indicates the variation and seasonal range of productivity over the year. The phase value determines the time of the peak of NDVI and hence the timing of most green-up. As a result, the phenological difference reflected by saltcedar and native vegetation

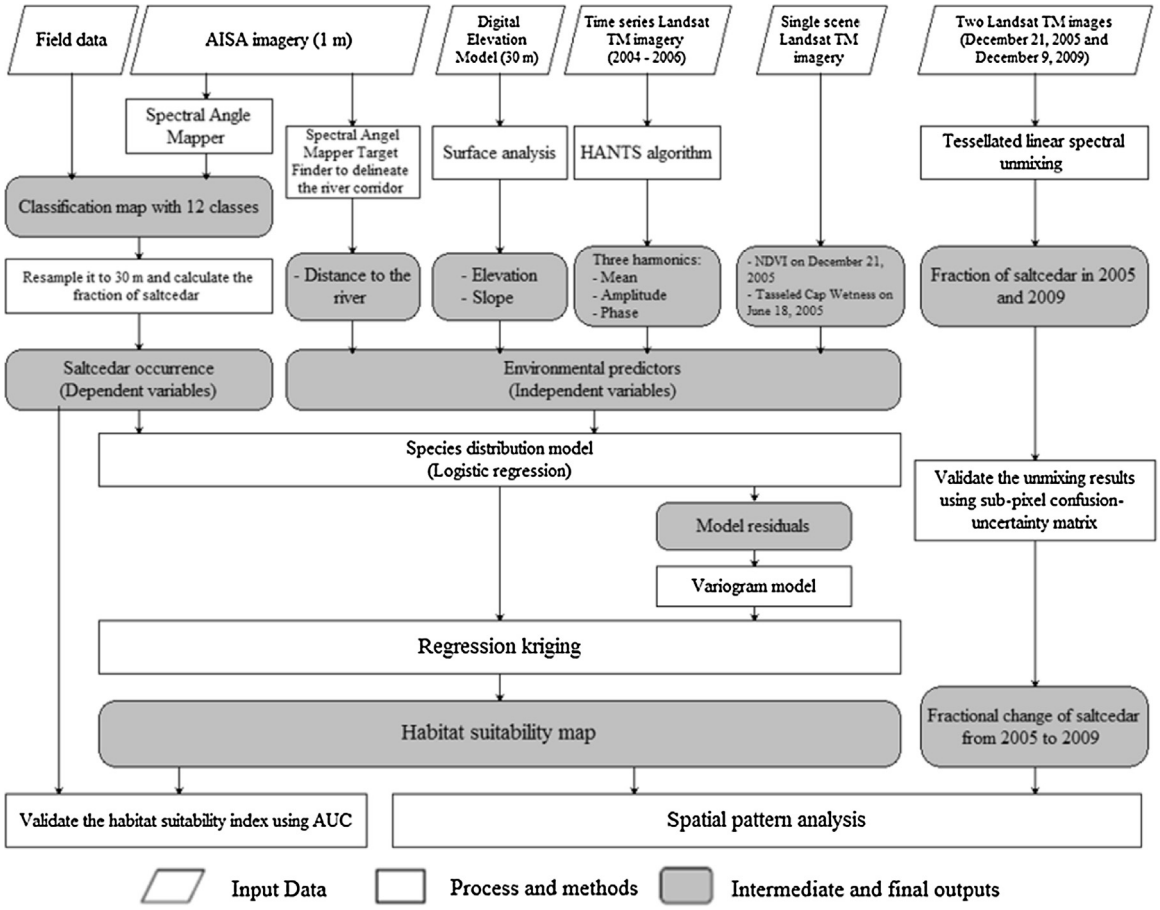

Fig. 3. A flow chart of major steps in mapping the suitable habitats of saltcedar with fine-resolution remote sensing.

can be captured by HANTS as environmental layers in subsequent mapping.

3.2. Logistic regression

Logistic regression was utilized in our study to analyze the influence of environmental drivers on the spatial distribution of saltcedar. As one of the classical SDMs, logistic regression relates the binary response of saltcedar with phenological attributes, vegetation indices and topographical features for obtaining the probability of the target response, as shown in Eq. (2) (Hosmer and Lemeshow, 2000).

$$p(Y) = \frac{1}{1 + \exp[-(\beta_0 + \beta_1 X_1 + \cdots + \beta_P X_P)]} \quad (2)$$

Here $X_1, \ldots, X_P$ denote the environmental factors and Y signifies the presence ($Y=1$) or absence ($Y=0$) of saltcedar. $\beta_1, \ldots, \beta_p$ are coefficients between the response variable and the corresponding environmental factor. $p(Y)$ indicates the habitat suitability of saltcedar ranging from 0 to 1. Therefore, with logistic regression approach, the location exhibiting vegetation and topographic characteristics similar to that of saltcedar occurrence will acquire higher probabilities in the habitat suitability mapping, or otherwise lower probabilities.

We applied the subset selection method with Akaike Information Criterion (AIC) to determine the significant environmental drivers in our fine scale mapping. AIC is defined as the minus twice the log likelihood of the fitted model plus two times the number of variables, and thus it can penalize the addition of variables to the model and compromise between model performance and complexity (Burnham and Anderson, 2002). Accordingly, AIC can identify the most parsimonious model, and the model with the lowest value of AIC will be finally selected.

3.3. Regression kriging

Spatial autocorrelation (SAC) is defined as the property of random variables with space, namely values of a variable are a function of proximity or distance, and positively or negatively correlated compared with randomly associated observations (Franklin, 2009; Legendre and Legendre, 1998). Thus a too-short sampling distance may include too many observations with similar attributes. It violates the assumption of traditional statistical methods, namely the distribution of vegetation is random and each observation is independent. Due to SAC, each observation contributes less information, standard errors tend to be underestimated with traditional hypothesis testing measures, and likelihood of type I errors (false positives) will increase (Franklin, 2009; Miller et al., 2007). Geostatistical methods, including kriging and variogram models, have been increasingly applied to characterize the spatial pattern of observations and quantify the degree of spatial dependence (Curran and Atkinson, 1998; Garrigues et al., 2007; Van der Meer, 2012; Woodcock et al., 1988). With the variogram model, residuals from the non-spatial regression can be mapped in order to determine whether a potential spatial autocorrelation problem exists (Arieira et al., 2011; Elith and Leathwick, 2009; Wagner and Fortin, 2005).

Regression kriging (RK), as a geostatistical interpolation method, assumes that model residuals have a spatial structure

caused by the biotic interaction or inaccurate predictors (Karl and Maurer, 2010; Meng et al., 2009; Miller et al., 2007). RK combines flexible regression models (e.g., GLMs, GAMs, and decision trees) for fitting the explanatory variation with simple kriging for interpolating the regression residuals, as shown in Eq. (3) (Hengl et al., 2007).

$$z(s_0) = y(s_0) + e(s_0) = y(s_0) + \sum_{i=1}^{n} \lambda_i e(s_i) \quad (3)$$

Here $z(s_0)$ is the predicted habitat suitability at location s_0 with consideration of both regression parts $y(s_0)$ and residual parts $e(s_0)$. $y(s_0)$ is the fitting value by logistic regression at s_0, as shown in Eq. (2). $e(s_0)$ is determined by the summation of weighted residuals $e(s_i)$, and λ_i is the kriging weight determined by the spatial structure. The processes for calculating RK include: (1) develop a logistic regression model relating the target response with environmental variables; (2) derive the residuals at all sample locations and check the distribution of residuals; (3) model the covariance structure of residuals with both directional and omnidirectional variograms; (4) interpolate the residuals using simple kriging with fitted variogram; (5) add the interpolated residuals to the regression surface at each prediction location.

3.4. Model validation

Receiver Operating Characteristic (ROC) curve analysis was used in our study to evaluate the performance of logistic regression and regression kriging model. A ROC curve is a plot of sensitivity (true positive) against 1-specificity (false positive) for all available probability thresholds (Fielding and Bell, 1997; Manel et al., 2002). Area under the curve (AUC) is derived by summing the area under the ROC curve and it ranges from 0.5 to 1.0. The higher value of AUC indicates better performance of the predictive model. An AUC value of 0.5 indicates that discriminating power is not better than random assignment, while an AUC value of 1.0 implies perfect discriminating power.

Additionally, we evaluated the performance and validity of SDMs in our study by investigating the fractional change of saltcedar from 2005 to 2009, with the expectation that it can provide us a new insight for validating the model from reality data (e.g. unmixing results) and developing more reliable models. Specifically, we obtained the fraction of saltcedar in both 2005 and 2009 by unmixing two Landsat TM images, and compared the fractional change of saltcedar to the habitat suitability index by calculating the average fractional change of saltcedar and the change of area occupied by saltcedar from 2005 to 2009 with all the pixels in both suitable and unsuitable areas. Two Landsat TM images were acquired on December 21, 2005 and on December 9, 2009. We assumed that suitable sites predicted by SDMs with good performance will cause a fraction increase and unsuitable areas will have a fraction decrease.

The fraction of saltcedar was calculated from Landsat TM images using tessellated linear spectral unmixing (TLSU) method (Silván-Cárdenas and Wang, 2010), in which the pixel can be linearly unmixed by the enclosing endmembers based on Delaunay tessellations. TLSU was implemented in Matlab and utilized the spectral library built from the AISA image based on the ground truth GPS points collected during the two field campaigns. VIF was utilized to quantify the level of multicollinearity in the endmembers (Van der Meer and Jia, 2012). All the VIF values calculated were less than 5, which indicated that no strong multicollinearity exists among the endmembers. By considering the intra-class variability, TLSU can produce a more accurate classification result than both unconstrained and constrained linear spectral unmixing methods (Silván-Cárdenas and Wang, 2010). Accuracy was assessed through the sub-pixel confusion-uncertainty matrix (SCM) suggested by Silván-Cárdenas and Wang (2008). Reference fractions in SCM were derived by aggregating the AISA classification result to the 30 m scale considering the intrinsic difficulties of collecting ground-truth fractional coverage data in the field. A total of 600 testing pixels were selected in the areas that do not have a significant change, so we can evaluate the unmixing results in 2005 and 2009 simultaneously.

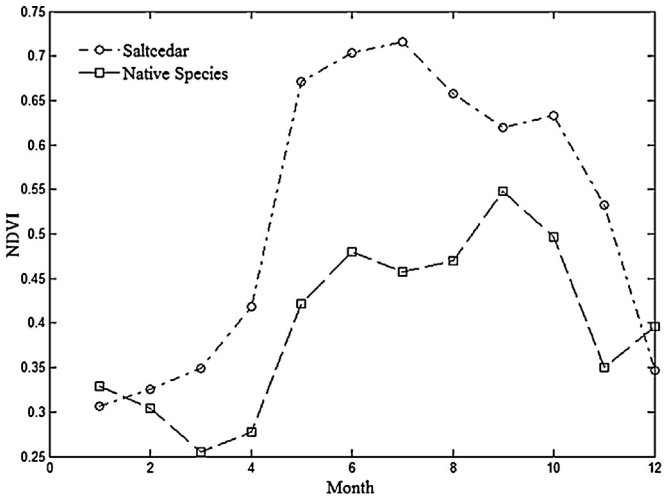

Fig. 4. The average intra-annual NDVI time series curve of saltcedar and native species.

4. Results

4.1. Harmonic characteristics

HANTS algorithm was implemented in our study to extract the phenological profile of the vegetation based on time series NDVI data. Pure pixels of both saltcedar and native vegetation, with the percentage greater than 95%, were located and decomposed from the resampled AISA classification images (30 m) respectively, and were then averaged for constructing the intra-annual time series curve (Fig. 4). The curve of saltcedar was dominated by the single annual pulse with the timing of peak green-up appearing in July, whereas the curve of native vegetation exhibited more complex signal with extended summer peak of NDVI occurring in June and August. Additionally, NDVI profile of saltcedar showed much stronger periodic characteristics than native vegetation. The variability of NDVI value of saltcedar within the year, ranging from 0.31 to 0.73, was much larger than that of native species, which varies from 0.28 to 0.51. The distinct seasonal patterns exhibited by NDVI time series curve were subsequently characterized by harmonic components.

Harmonic characteristics of saltcedar and native vegetation were shown in Figs. 5 and 6 respectively. With regard to the unimodal periodic pattern exhibited in the NDVI profile, the first harmonic of saltcedar captures most of the temporal variability and has a much higher amplitude value (0.21) compared to the successive terms. The corresponding phase, which illustrates the timing of maximum NDVI, occurs in July, and is finely tuned by the second and third harmonic. However, as for native species, the predominant first harmonic has the amplitude of 0.12 with the phase value appearing in August. Despite the strong summer-peak greenness pattern, the NDVI profile of native vegetation differs from the unimodal pattern exhibited by the saltcedar, since it has a relatively high third harmonic term compared to the second one, and tends to produce the extended or secondary periodicity in greenness during the summer. Additionally, for both saltcedar and native species, we

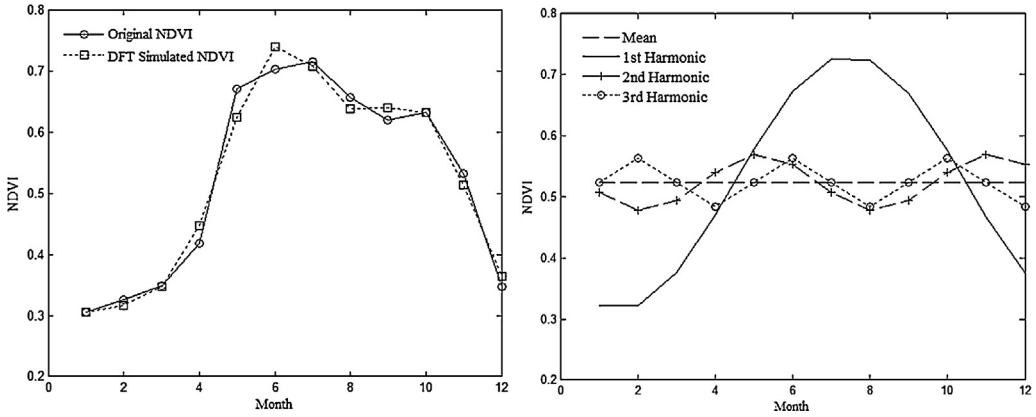

Fig. 5. The raw NDVI time series profile of saltcedar and the simulated curve by summing the mean value and first three harmonics (left). Decomposed mean value and first three harmonic terms for saltcedar (right).

found the simulated NDVI time series curves by summing all the harmonic components (Figs. 5 and 6), fit the original NDVI profile quite well.

By comparing the NDVI phenological profile of saltcedar with that of native vegetation, we found that the most significant differences existed in the mean, the first and third harmonic of decomposed time-series components. Accordingly, six pixel-based environmental layers, namely the mean NDVI, the amplitude and phase of first harmonic, and the amplitude and phase of third harmonic, were produced and utilized in the subsequent fine-scale mapping.

Table 1
The best subset selected for the logistic regression model.

Environmental variables	Coefficients	Standard error	Significance
Distance to the river	−0.021	0.009	0.001
3rd Harmonic_Phase	−0.592	0.119	0.001
1st Harmonic_Amplitude	12.564	3.774	0.002
TC_Wetness_June_18	15.555	5.530	0.005
Elevation	−0.045	0.021	0.036
Constant	−41.701	18.619	0.025

4.2. Logistic regression result

In total, there were ten environmental variables considered in the logistic regression model, namely the mean NDVI, the amplitude and phase of first harmonic, the amplitude and phase of third harmonic, the single-scene NDVI in December, the tasseled cap wetness in June, distance to the river, slope and elevation. All environmental variables were assessed for collinearity through Pearson correlation tests and variance inflation function (VIF) diagnostics (Davis et al., 1986). We found that all Pearson's correlation coefficients between environmental variables had the absolute value less than 0.6 and the highest VIF score for a variable was 2.87, indicating a negligible collinearity effect. Hence, all the variables were considered for the subsequent best subset selection procedure. Through minimizing the AIC value, the best fitted model with five significant environmental factors was selected (Table 1). Therefore, our final model included elevation, the distance to the river, the amplitude of the first harmonic, the phase of the third harmonic and the tasseled cap wetness in June. In this scenario the AIC value was lowest with the value of 320.34.

Among all the environmental variables, the distance to the river is regarded as the most significant variable in identifying the suitable habitat of saltcedar. This outcome is supported by the previous studies that the germination of saltcedar requires the extended moisture and the densest stands of saltcedar tend to locate along the river bank (Di Tomaso, 1998; Frazier and Wang, 2011; Warren and Turner, 1975). Jarnevich et al. (2011) also observed that the distance to the river is the strongest predictor in mapping the habitat suitability of saltcedear at the national scale. Another important topographical factor is elevation, as the expansion rate of saltcedar is limited by local elevation and it spreads very slowly after 1220 m (Zavaleta and Royval, 2002). Additionally, the amplitude of first harmonic is preferred by the model with its ability to distinguish the seasonal variation of productivity over the year. The phase of third harmonic is also selected by allowing for the detection of the

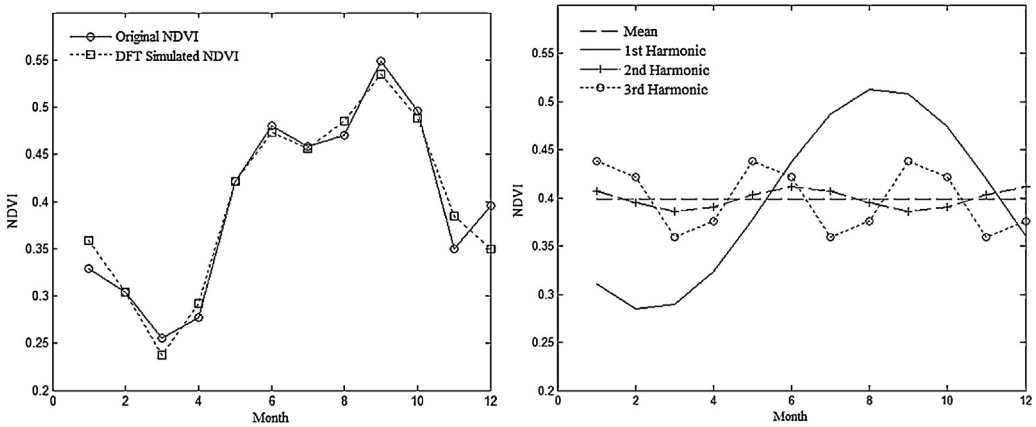

Fig. 6. The raw NDVI time series profile of native species and the simulated curve by summing the mean value and first three harmonics (left). Decomposed mean value and first three harmonic terms for native species (right).

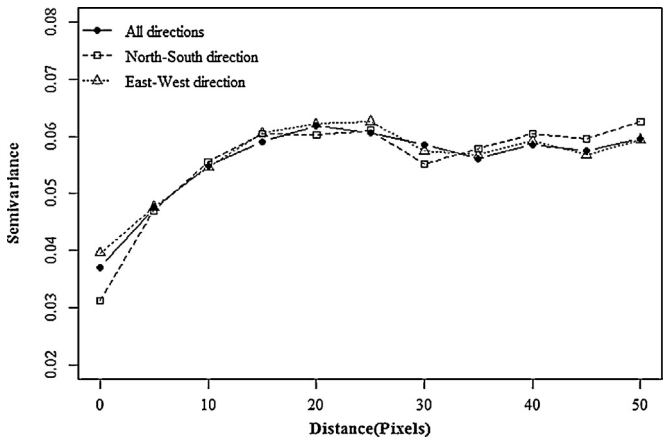

Fig. 7. North-south directional, east-west directional, and omnidirectional variograms of residuals of the logistic regression model.

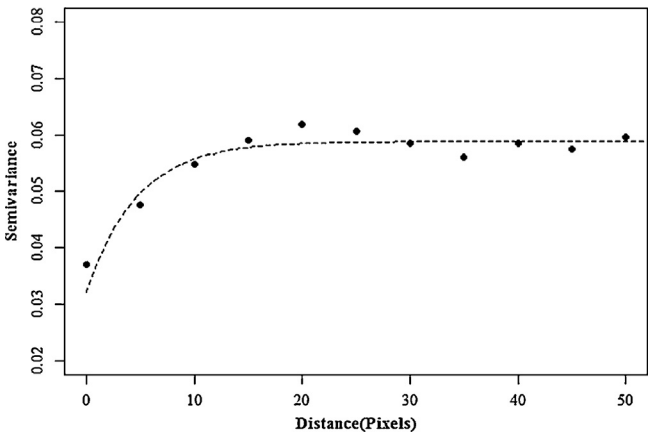

Fig. 8. Sample omnidirectional variogram of residuals of the logistic regression model fitted with the Matern model.

extended or secondary periodicity in greenness, as illustrated in Section 4.1. Lastly, tasseled cap wetness in June also exerts a role in our fine scale mapping probably owing to the unique signature exhibited by saltceder in June, when it achieves the peak in green-up and yields purple-pink flowers (Evangelista et al., 2009).

AUC value was utilized in our fine-scale model for evaluating the model performance. With our testing samples, AUC value calculated was 0.902 and it was categorized into the excellent level in terms of the discriminating power. Therefore, the logistic regression model, with five environmental predictors selected, exhibits good performance in predicting the suitable habitat of saltcedar in our study area.

4.3. Spatial autocorrelation

After normalizing the residuals of training points derived from logistic regression, we calculated both directional and omnidirectional semivariance of residuals in order to detect anisotropy in point patterns (Fig. 7). Directional variograms were calculated in a north-south and an east-west direction with an angular tolerance of $\pm 45^{\circ}$, and they showed little variation compared to the omnidirectional variogram. Therefore, only the isotropic variogram representing the overall spatial pattern of residuals was considered in our study. The isotropic variogram was then fitted by ordinary least square approach and the best-fitting parametric model with minimum root mean square errors was the Matern model (Fig. 8), where the partial sill was 0.037, the nugget effect was 0.021, the range was 13.98 and the kappa was 0.5. The nugget to sill ratio was approximately 36% and it indicated that about 64% of the variation was caused by the spatial pattern. As displayed in Fig. 8, the difference of sampled points continuously increased with the separation distance until it flattened out at a distance of 13.98 pixels. It implied that observations closer than the range were spatially autocorrelated and locations further apart beyond the distance of 420 m were not. With the semivariogram model, the kriging weights were calculated by minimizing the variance of prediction errors. Simple kriging was subsequently employed to interpolate the surface from the residuals.

While logistic regression model provided a means to estimate the global trend of the habitat suitability, simple kriging method allowed for local deviation from the mean by incorporating the spatial structure of residuals. We found that AUC value for validating the regression kriging method increased from 0.902 to 0.933, and hence incorporating the spatial autocorrelation tended to improve the model performance at our fine-scale mapping. To illustrate the spatial prediction difference, we produced binary maps of saltcedar based on the optimum probability threshold (Miller, 2005) for both logistic regression and regression kriging model (Fig. 9). Through locating the testing points on both maps, we found that several locations of absence, which were previously predicted as presence by logistic regression, were corrected by regression kriging model. As shown in Fig. 9, the yellow dots denoting the absence in the green box area were more likely to be predicted correctly by the regression kriging model. With regard to presence points, the omission error was quite small and most points were predicted equally by both methods.

4.4. Spatial pattern analysis

With the five environmental factors selected, the habitat suitability index was calculated with the regression kriging model for the whole study area. In the habitat suitability map (Fig. 10), the red color denotes the highly suitable area and the blue color indicates the unsuitable area for the establishment of saltcedar. As shown in Fig. 10, upper reaches of study areas are more vulnerable to saltcedar invasion and the predicted suitable habitats are mostly distributed along the river. Overall, a great portion of study area is susceptible to saltcedar invasion and highly suitable areas are critically important for local governors to conduct timely ground reconnaissance and develop corresponding control methods.

We evaluated the performance and validity of SDMs in our study by investigating the fractional change of saltcedar from 2005 to 2009. Based on TLSU methods, the fractions of saltcedar in both 2005 and 2009 were calculated at the scale of 30 m (Fig. 10). The overall accuracy of saltcedar abundances calculated from sub-pixel confusion-uncertainty matrix was 81.7% for the 2005 unmixing result and 83.4% for the year 2009. Given the relatively high accuracy of unmixing results, we calculated the fractional change of saltcedar from 2005 to 2009, and compared it to the habitat suitability index in our whole study area. For these suitable locations, we found that the average fractional change of saltcedar was 0.17 from 2005 to 2009, and the area occupied by saltcedar increased from 3.79 km^2 to 5.47 km^2. For the unsuitable ones, the average fractional change of saltcedar was −0.03 from 2005 to 2009, and the area occupied by saltcedar decreased from 1.48 km^2 to 1.13 km^2. The comparison result corroborated the good performance of the model. It indicated that saltcedar were spreading across our study site, and the area occupied by saltcedar in 2009 increased dramatically compared with that in 2005. Through comparing the habitat suitability index with the spatial pattern change of saltcedar from 2005 to 2009, we discovered that several suitable locations of saltcedar encountered a fractional increase, such as the areas denoted by yellow dashed circles in Fig. 10. Overall,

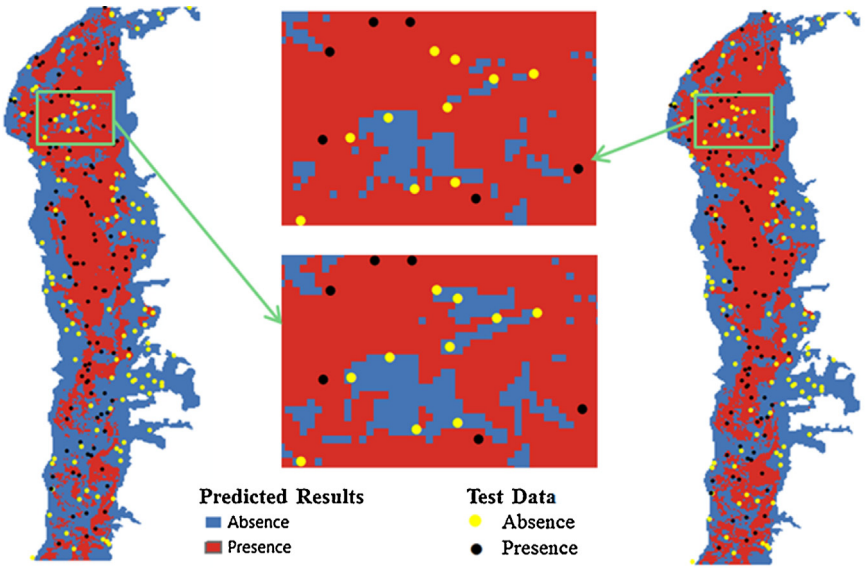

Fig. 9. Comparison of predicted suitable habitats of saltcedar using regression kriging model (left) and logistic regression model (right) with detailed testing points.

the spreading pattern of saltcedar in our study coincided with the suitability index predicted by our model. By monitoring the fractional and spatial-temporal dynamic change of saltcedar, we attempted to provide a new insight for validating the SDMs from reality under the pixel-based equilibrium assumption of SDMs.

5. Discussion

Phenological attributes summarized by the harmonic analysis reflected the seasonal dynamics of vegetation with respect to the photosynthetic activity. Through extracting the phenological profile of both saltcedar and native vegetation with the intra-annual time series data, we found that saltcedar expressed greater temporal variability and showed stronger periodic characteristics than native vegetation. The variability of productivity of saltcedar was mostly explained by the first harmonic, and the temporal profile of saltcedar exhibited a single annual pulse with the timing of maximum productivity appearing in July. The timing of dominant peak greenness in the mid-summer, and leaf senescence in the late fall and early winter reflected by decreased NDVI, are consistent with the previous studies (Cord et al., 2010; Everitt and Deloach, 1990; Everitt et al., 1996). However, for the native species, the temporal variability was captured by both the first and third harmonics, and the NDVI curve showed more extended peak of greenness during the summer. The phenological difference reflected by saltcedar and native species indicates the possibility of distinguishing saltcedar with time-series Landsat TM images. Though time-series analysis has been proven useful and efficient in mapping the distribution of saltcedar (Evangelista et al., 2009; Morisette et al., 2006), the intra-annual NDVI phenological attributes of both saltcedar and native vegetation have not been studied before. Therefore, this study was the first instance of exploiting the time series phenological difference of saltcedar and associated vegetation.

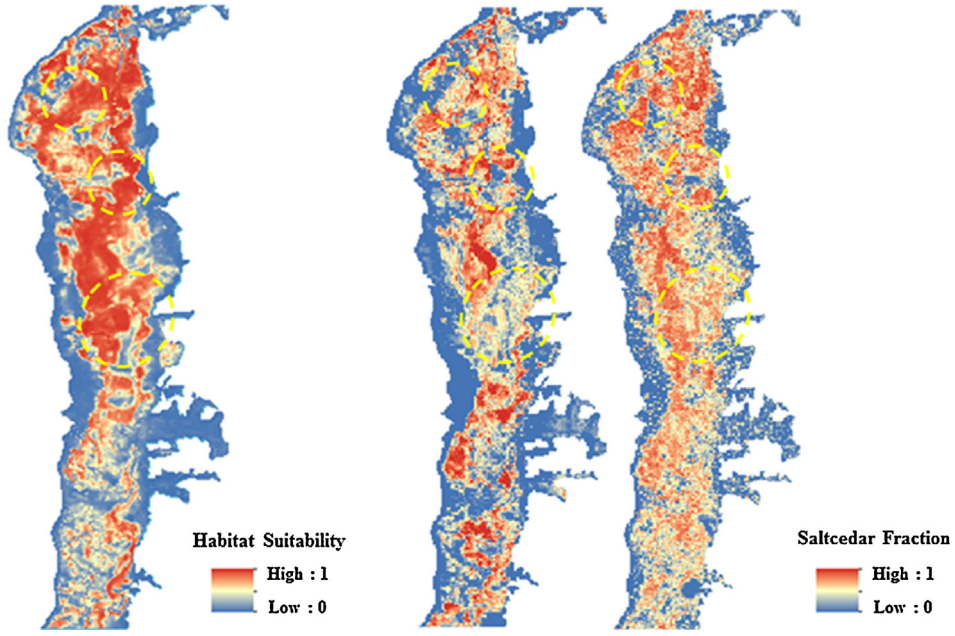

Fig. 10. Comparison of the agreement between the habitat suitability index (left) and the fractional change of saltcedar from 2005 (middle) to 2009 (right).

Remote sensing images, through providing both environmental predictors and species occurrence data, dramatically facilitated the fine-scale mapping of habitat suitability. In the case of SDMs, most studies were conducted at regional to national scales. At such coarse scales, bioclimatic predictors were usually regarded as significant in detecting suitable habitats as well as forecasting the species vulnerability to climate change. However, SDMs depending only on climate predictors can produce only a very rough approximation of species distributions. Fine-scale predictors were therefore necessarily important to uncover the detailed spatial pattern of habitats. In our study several fine-scale predictors, including phenological attributes, vegetation indices and topographical features, were explored with remotely sensed images. These remote sensing-based fine-scale predictors can quantify the spatial heterogeneity in landscape, and locate more appropriate areas susceptible to invasion by saltcedar, which partially explained the good performance of fine-scale SDM in our case. Another challenge in SDMs is the lack of sufficient numbers of occurrence data. Advances in remote sensing technologies can overcome this limitation to a certain extent by making it plausible for classifying the species at different scales, and thus obtaining more flexible and randomized occurrence records. In this study we acquired the occurrence data by using 10% as the threshold for categorizing the resampled AISA fraction image into presence and absence. Results indicated that the model we developed with remote sensing-based occurrence data achieved a good performance in our study area. Due to the disconnect between remote sensing specialists and ecologists, occurrence data were seldom acquired from remote sensing images before (Turner et al., 2003). Clearly, there is a great promise for future studies on incorporating classification or spectral unmixing results at the species level into SDMs, and identifying the optimal threshold for tackling early detection and equilibrium assumption problems in modeling the distribution of invasive species.

Regression kriging combines the flexible regression models for fitting the explanatory variation with simple kriging for interpolating the regression residuals. By mapping the residuals of regression model with variogram-based methods, the spatial structure caused by the unmeasured biotic process and inaccurate predictor variables can be incorporated. In our fine-scale mapping, interpolated residuals by the simple kriging compensated for local factors and improved model accuracy with AUC value increasing from 0.902 to 0.933. Spatial autocorrelation of residuals can be detected within about 420 m of sample points. Due to the data limit and scale difference in previous studies, this was the first instance of considering spatial autocorrelation in modeling the suitable habitats of saltcedar. The significance of incorporating the spatial autocorrelation can also be investigated at different scales. Besides, other spatial autocorrelation methods, including autoregressive methods, parameter estimation methods and geographically weighted regression, can be compared under different sampling campaigns for testing the role of spatial autocorrelation in species distribution model.

Validation of habitat suitability of invasive species can also benefit from the knowledge of reality, other than traditional statistical methods (e.g. AUC), owing to the characteristic of potential infestation. Based on spectrally unmixed images, we investigated the fractional change of saltcedar from 2005 to 2009, and found that the general spreading pattern of saltcedar coincided with the suitability index predicted by the model (Fig. 10). The habitat suitability index of invasive species calculated by SDMs indicates the potential distribution of species, and reflects the trend of spatial-temporal dynamic change of species in reality. Through monitoring the dynamic change of invasive species over time, the potentially rapid repeat interval of remote sensing images suggests a very promising approach for validating the habitat suitability. In this study, we provided a new insight for validating the SDMs from unmixing results by calculating the average fractional change of saltcedar and the change of area occupied by saltcedar from 2005 to 2009, which represents an initial effort for us to go beyond AUC to examine the model's performance in capturing the spatial patterns of potential suitable locations. Other quantitative methods can also be investigated in future studies for enhancing our understanding of validating modeled suitability with reality data derived from remote sensing.

Compared with the areas that saltcedar now occupies, the suitability map indicates that there are much greater areas susceptible to saltcedar invasion. Most of these areas are distributed along the river, and this fact emphasizes the role of distance to the river in fine-scale habitat suitability mapping. Prior research suggests that we are still in the early stage of saltcedar invasion (Cord et al., 2010; Morisette et al., 2006). Therefore, owing to its ability to provide detailed habitat suitability information, fine scale mapping driven by remote sensing images can dramatically help local governors forecast the invasive potential of saltcedar and develop corresponding proactive control methods. With the increasing availability of remote sensing images, we believe that fine-scale mapping of habitat suitability can be easily extended to other study areas and it will be beneficial for us to understand the invasion process as well as develop effective management strategies.

6. Conclusions

Based on the niche concept, species distribution model represents an appealing tool for identifying the suitable habitats susceptible to saltcedar invasion. In this study, we exploit several fine-scale resolution environmental variables through remote sensing images, with the expectation of uncovering the detailed spatial pattern and predicting the early invasion of saltcedar. At a scale of 30 m, pixel-based environmental variables we selected include vegetation indices, time-series phenological information and topographical features. Among ten environmental variables, the distance to the river, the NDVI phase of the third harmonic, and the NDVI amplitude of the first harmonic are regarded as the most significant in identifying the suitable habitat of saltcedar. Spatial autocorrelation can be detected within about 420 m of sample points. Incorporating the spatial autocorrelation of residuals can improve the model performance with the AUC value increasing from 0.902 to 0.933 in our study site. Our results also indicate that harmonic components extracted from NDVI time series profile can represent the phenological characteristics at the species level, and the phenological difference reflected by saltcedar and native species indicates the possibility of distinguishing saltcedar with time-series Landsat TM images. Another important finding in this study is that the area of suitable habitat susceptible to saltcedar invasion is much larger than that is currently invaded. Highly suitable areas for the establishment of saltcedar are mainly distributed along the river, and saltcedar tends to spread across our study site and invade more areas over time.

Since we are still in the early stage of saltcedar infestations, predicting the habitat suitability and locating appropriate areas at high risk of infestation are critically important for local governors to conduct timely ground reconnaissance and develop corresponding control methods. Through uncovering the detailed spatial pattern and quantifying the spatial heterogeneity, fine scale mapping driven by remote sensing images can dramatically help local governors forecast the invasive potential of saltcedar. As remote sensing images become more readily available, we believe that fine-scale mapping of habitat suitability can be easily generalized and extended to other areas.

There are several avenues of future research offered by this study. For instance, we selected 10% as the threshold for

categorizing the fractional coverage of resampled AISA image into presence and absence. Future work can include the analysis of selecting the optimal threshold for the binary division of occurrence data. Additionally, the mechanism driving the phenological difference of saltcedar and associated native vegetation, the significance of incorporating the spatial autocorrelation at different scales, and the validity of evaluating the agreement between habitat suitability and fractional changes over a continuous period, can all be further investigated to produce more accurate predictions and facilitate the generalization of fine-scale mapping of habitat suitability.

References

Andrew, M.E., Ustin, S.L., 2009. Habitat suitability modelling of an invasive plant with advanced remote sensing data. Diversity and Distributions 15, 627–640.

Arieira, J., Karssenberg, D., Jong, S.d., Addink, E., Couto, E., Nunes da Cunha, C., Skøien, J., 2011. Integrating field sampling, geostatistics and remote sensing to map wetland vegetation in the Pantanal, Brazil. Biogeosciences 8, 667–686.

Borcard, D., Legendre, P., 2002. All-scale spatial analysis of ecological data by means of principal coordinates of neighbour matrices. Ecological Modelling 153, 51–68.

Briggs, W., Henson, V., 1995. The DFT: An Owner's Manual for the Discrete Fourier Transform. Society for Industrial and Applied Mathematics, Philadelphia.

Burnham, K.P., Anderson, D.R., 2002. Model Selection and Multi-Model Inference: A Practical Information-Theoretic Approach. Springer, New York, NY.

Canty, M.J., 2007. Image Analysis, Classification and Change Detection in Remote Sensing: With Algorithms for ENVI/IDL. CRC, Boca Raton, FL.

Canty, M.J., Nielsen, A.A., 2008. Automatic radiometric normalization of multitemporal satellite imagery with the iteratively re-weighted MAD transformation. Remote Sensing of Environment 112, 1025–1036.

Carruthers, R.I., Deloach, C.J., 2004. Progress on the Biological Control of Tamarisk, Cal-IPC News. California Invasive Plant Council (Cal-IPC), Berkeley, CA.

Cohen, W.B., Spies, T.A., Fiorella, M., 1995. Estimating the age and structure of forests in a multi-ownership landscape of western Oregon, USA. Remote Sensing 16, 721–746.

Cord, A., Klein, D., Dech, S., 2010. Remote sensing time series for modeling invasive species distribution: a case study of *Tamarix* spp. in the US and Mexico. In: International Environmental Modeling and Software Society (iEMSs), Fifth Biennial Meeting.

Curran, P.J., Atkinson, P.M., 1998. Geostatistics and remote sensing. Progress in Physical Geography 22, 61–78.

Davis, C., Hyde, J., Bangdiwala, S., Nelson, J., 1986. An example of dependencies among variables in a conditional logistic regression. In: Modern Statistical Methods in Chronic Disease Epidemiology., pp. 140–147.

Del Barrio, G., Harrison, P., Berry, P., Butt, N., Sanjuan, M., Pearson, R., Dawson, T., 2006. Integrating multiple modelling approaches to predict the potential impacts of climate change on species' distributions in contrasting regions: comparison and implications for policy. Environmental Science & Policy 9, 129–147.

Di Tomaso, J.M., 1998. Impact, biology, and ecology of saltcedar (*Tamarix* spp.) in the southwestern United States. Weed Technology, 326–336.

Elith, J., Leathwick, J.R., 2009. Species distribution models: ecological explanation and prediction across space and time. Annual Review of Ecology, Evolution, and Systematics 40, 677–697.

Engler, R., Guisan, A., Rechsteiner, L., 2004. An improved approach for predicting the distribution of rare and endangered species from occurrence and pseudo-absence data. Journal of Applied Ecology 41, 263–274.

Evangelista, P.H., Kumar, S., Stohlgren, T.J., Jarnevich, C.S., Crall, A.W., Norman III, J.B., Barnett, D.T., 2008. Modelling invasion for a habitat generalist and a specialist plant species. Diversity and Distributions 14, 808–817.

Evangelista, P.H., Stohlgren, T.J., Morisette, J.T., Kumar, S., 2009. Mapping invasive tamarisk (*Tamarix*): a comparison of single-scene and time-series analyses of remotely sensed data. Remote Sensing 1, 519–533.

Everitt, J., Deloach, C., 1990. Remote sensing of Chinese tamarisk (*Tamarix chinensis*) and associated vegetation. Weed Science, 273–278.

Everitt, J.H., Escobar, D.E., Alaniz, M.A., Davis, M.R., Richerson, J.V., 1996. Using spatial information technologies to map Chinese tamarisk (*Tamarix chinensis*) infestations. Weed Science, 194–201.

Ficetola, G.F., Thuiller, W., Miaud, C., 2007. Prediction and validation of the potential global distribution of a problematic alien invasive species – the American bullfrog. Diversity and Distributions 13, 476–485.

Fielding, A.H., Bell, J.F., 1997. A review of methods for the assessment of prediction errors in conservation presence/absence models. Environmental Conservation 24, 38–49.

Franklin, J., 2009. Mapping Species Distributions: Spatial Inference and Prediction. Cambridge University Press, Cambridge, UK.

Frazier, A., Wang, L., 2011. Characterizing spatial patterns of invasive species using sub-pixel classifications. Remote Sensing of Environment 115, 1997–2007.

Friedman, J.M., Auble, G.T., Shafroth, P.B., Scott, M.L., Merigliano, M.F., Freehling, M.D., Griffin, E.R., 2005. Dominance of non-native riparian trees in western USA. Biological Invasions 7, 747–751.

Garrigues, S., Allard, D., Baret, F., 2007. Using first- and second-order variograms for characterizing landscape spatial structures from remote sensing imagery. Geoscience and Remote Sensing, IEEE Transactions on 45, 1823–1834.

Gottschalk, T.K., Aue, B., Hotes, S., Ekschmitt, K., 2011. Influence of grain size on species–habitat models. Ecological Modelling 222, 3403–3412.

Groeneveld, D.P., Watson, R.P., 2008. Near-infrared discrimination of leafless saltcedar in wintertime Landsat™. International Journal of Remote Sensing 29, 3577–3588.

Hamada, Y., Stow, D.A., Coulter, L.L., Jafolla, J.C., Hendricks, L.W., 2007. Detecting Tamarisk species (*Tamarix* spp.) in riparian habitats of Southern California using high spatial resolution hyperspectral imagery. Remote Sensing of Environment 109, 237–248.

Hengl, T., Heuvelink, G., Rossiter, D.G., 2007. About regression-kriging: from equations to case studies. Computers & Geosciences 33, 1301–1315.

Hosmer, D.W., Lemeshow, S., 2000. Applied Logistic Regression. Wiley-Interscience, New York, NY.

Jakubauskas, M.E., Legates, D.R., Kastens, J.H., 2001. Harmonic analysis of time-series AVHRR NDVI data. Photogrammetric Engineering and Remote Sensing 67, 461–470.

Jarnevich, C.S., Evangelista, P., Stohlgren, T.J., Morisette, J., 2011. Improving national-scale invasion maps: tamarisk in the western United States. Western North American Naturalist 71, 164–175.

Jin, S., Sader, S.A., 2005. Comparison of time series tasseled cap wetness and the normalized difference moisture index in detecting forest disturbances. Remote Sensing of Environment 94, 364–372.

Karl, J.W., Maurer, B.A., 2010. Spatial dependence of predictions from image segmentation: a variogram-based method to determine appropriate scales for producing land-management information. Ecological Informatics 5, 194–202.

Kerns, B.K., Naylor, B.J., Buonopane, M., Parks, C.G., Rogers, B., 2009. Modeling tamarisk (*Tamarix* spp.) habitat and climate change effects in the northwestern United States. Invasive Plant Science and Management 2, 200–215.

Kruse, F., Lefkoff, A., Boardman, J., Heidebrecht, K., Shapiro, A., Barloon, P., Goetz, A., 1993. The spectral image processing system (SIPS) – interactive visualization and analysis of imaging spectrometer data. Remote Sensing of Environment 44, 145–163.

Legendre, P., Legendre, L., 1998. Numerical Ecology. Elsevier Science & Technology, Amsterdam, The Netherlands.

Manel, S., Williams, H.C., Ormerod, S.J., 2002. Evaluating presence–absence models in ecology: the need to account for prevalence. Journal of Applied Ecology 38, 921–931.

Meng, Q., Cieszewski, C., Madden, M., 2009. Large area forest inventory using Landsat ETM+: a geostatistical approach. ISPRS Journal of Photogrammetry and Remote Sensing 64, 27–36.

Menke, S., Holway, D., Fisher, R., Jetz, W., 2008. Characterizing and predicting species distributions across environments and scales: Argentine ant occurrences in the eye of the beholder. Global Ecology and Biogeography 18, 50–63.

Miller, J., 2005. Incorporating spatial dependence in predictive vegetation models: residual interpolation methods. The Professional Geographer 57, 169–184.

Miller, J., Franklin, J., Aspinall, R., 2007. Incorporating spatial dependence in predictive vegetation models. Ecological Modelling 202, 225–242.

Moody, A., Johnson, D.M., 2001. Land-surface phenologies from AVHRR using the discrete Fourier transform. Remote Sensing of Environment 75, 305–323.

Morisette, J.T., Jarnevich, C.S., Ullah, A., Cai, W., Pedelty, J.A., Gentle, J.E., Stohlgren, T.J., Schnase, J.L., 2006. A tamarisk habitat suitability map for the continental United States. Frontiers in Ecology and the Environment 4, 11–17.

Nielsen, A.A., 2007. The regularized iteratively reweighted MAD method for change detection in multi-and hyperspectral data. IEEE Transactions on Image Processing 16, 463–478.

Roerink, G., Menenti, M., Verhoef, W., 2000. Reconstructing cloudfree NDVI composites using Fourier analysis of time series. International Journal of Remote Sensing 21, 1911–1917.

Silván-Cárdenas, J., Wang, L., 2008. Sub-pixel confusion-uncertainty matrix for assessing soft classifications. Remote Sensing of Environment 112, 1081–1095.

Silván-Cárdenas, J., Wang, L., 2010. Retrieval of subpixel *Tamarix* canopy cover from Landsat data along the Forgotten River using linear and nonlinear spectral mixture models. Remote Sensing of Environment 114, 1777–1790.

Turner, W., Spector, S., Gardiner, N., Fladeland, M., Sterling, E., Steininger, M., 2003. Remote sensing for biodiversity science and conservation. Trends in Ecology & Evolution 18, 306–314.

Van der Meer, F., 2012. Remote-sensing image analysis and geostatistics. International Journal of Remote Sensing 33, 5644–5676.

Van der Meer, F.D., Jia, X., 2012. Collinearity and orthogonality of endmembers in linear spectral unmixing. International Journal of Applied Earth Observation and Geoinformation 18, 491–503.

Wagner, H.H., Fortin, M.J., 2005. Spatial analysis of landscapes: concepts and statistics. Ecology 86, 1975–1987.

Wang, L., Silvan, J., Yang, J., Frazier, A., 2013. Invasive saltcedar spread mapping using multi-resolution remote sensing data. Professional Geographer 65, 1–15.

Warren, D.K., Turner, R.M., 1975. Saltcedar (*Tamarix chinensis*) seed production, seedling establishment, and response to inundation. Journal of the Arizona Academy of Science 10, 135–144.

Woodcock, C.E., Strahler, A.H., Jupp, D.L., 1988. The use of variograms in remote sensing. I. Scene models and simulated images. Remote Sensing of Environment 25, 323–348.

Zavaleta, E.S., Royval, J.L., 2002. Climate change and the susceptibility of US ecosystems to biological invasions: two cases of expected range expansion. In: Schneider, S.H., Root, T.L. (Eds.), Wildlife Responses to Climate Change. Island Press, Washington, DC, USA, pp. 277–341.